INTERNATIONAL SOCIETY FOR SOIL MECHANICS AND GEOTECHNICAL ENGINEERING

SIMSG ISSMGE

This paper was downloaded from the Online Library of the International Society for Soil Mechanics and Geotechnical Engineering (ISSMGE). The library is available here:

https://www.issmge.org/publications/online-library

This is an open-access database that archives thousands of papers published under the Auspices of the ISSMGE and maintained by the Innovation and Development Committee of ISSMGE.

The paper was published in the proceedings of the 10th International Conference on Scour and Erosion and was edited by John Rice, Xiaofeng Liu, Inthuorn Sasanakul, Martin McIlroy and Ming Xiao. The conference was originally scheduled to be held in Arlington, Virginia, USA, in November 2020, but due to the COVID-19 pandemic, it was held online from October 18th to October 21st 2021.

Observation of progressive internal erosion in soils using X-ray CT scanner

Shintaro Nohara[1]

[1]Central Research Institute of Electric Power Industry, 1646 Abiko, Abiko-shi, Chiba-ken, Japan; e-mail: nohara-s@criepi.denken.or.jp Corresponding author.

ABSTRACT

Progressive internal erosion in soils was observed by conducting 1D column tests with multistep water injection. Two types of sand materials, fine sand (0.10-0.30 mmm of soil particle diameter) and a mixture material of fine sand and gravel (2–3 mm of soil particle diameter), were used in experiments to study their differences in internal erosion. The column was scanned after water injection using a microfocus X-ray CT scanner to visualize the change in soil structures. The progress of internal erosion was quantitatively evaluated using image analysis, such as gray value analysis and gravel-fabric analysis from CT images.

1. INTRODUCTION

Seepage failure is the internal erosion of soils caused by the accumulation of groundwater flow and transportation of soil particles. It is also referred to as piping and has several causes, including heterogeneous permeability, catchment topography of groundwater, dying plant roots, and activity of underground animals. Piping under the river levee or in earth dams can cause settlement or collapse of the ground structure and trigger extensive damage by flooding (Richard, 2007). Therefore, piping plays an important role in the safety assessment of river levees and earth dams. Further, the piping phenomenon plays an important role in the instability of natural slopes (Pierson, 1983). Several reports in the geo-disaster field of natural slopes caused by heavy rain indicated the presence of piping holes.

Previous studies performed on piping have employed 1D columns or 2D tanks made of acrylic glass in the laboratory to observe the soil material within from an outside viewpoint (Ke, 2012; Wang, 2016; Yang, 2017). However, piping is a complex phenomenon. Therefore, we must visualize it in soil materials and observe the progression of piping. For these reasons, we investigated piping progression behavior in soils using a microfocus X-ray CT scanner. In recent days, X-ray CT method has become an effective in obtaining the three-dimensional internal structure of geomaterials for observation without cutting or disturbing the objects. Especially, digital images with high-spatial resolution can be acquired using a micro-focused X-ray CT. For these reasons, X-ray CT technology is utilized in the field of geosciences (Ketcham, 2001; Otani, 2003; Desrues, 2006; Cnudde, 2013).

2. EXPERIMENTAL METHOD

2.1 MATERIALS

We used two kinds of soil materials. Sample1 comprised fine sand material with a particle diameter of 0.1–0.3 mm, whereas Sample2 was a mixture of fine sand and gravel with a particle diameter of 1–2 mm. The mixture ratio of fine sand to gravel was 80: 20 by weight. The soil particle densities of fine sand and gravel were 2.45 g/cm^3 and 2.57 g/cm^3, respectively. The soil particle size distribution curves of fine sand and gravel are shown in **Figure 1**.

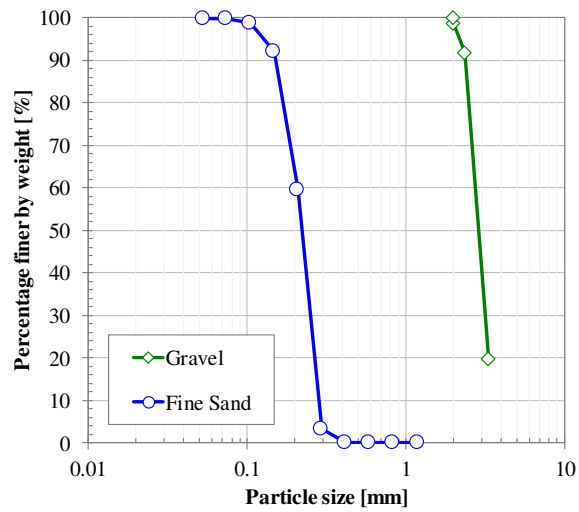

Figure 1. Particle size distribution curve

2.2 EXPERIMENTAL PROCEDURE

A schematic representation of the experimental apparatus is shown in **Figure 2**. The major steps of the experiment were as follows:

1) **Preparation of soil sample:**
First, a dry soil sample was prepared. In Sample2, fine sand and gravel were mixed completely before being compacted into the 1D column. Subsequently, the soil sample was compacted and divided into six layers in the 1D column (60 mm internal diameter and 200 mm height) made of acrylic glass. The dry density was 1.45 g/cm^3 and the porosity was 0.41. The thickness of each soil layer was 20 mm. Gravel filters were placed at the upper and lower parts of the soil to prevent soil particles from flowing into the pump. The thickness of each gravel filter is 40 mm. The gravel was the same which used of gravel filter as shown in **Figure 1**.
2) **Saturation of soil sample:**
De-aired water was injected at 2 mL/min using an HPLC pump at the lower part of the column for more than five days.
3) **CT scan before water injection:**
The column was scanned using a microfocus X-ray CT scanner before water injection.
4) **Preparation of measuring device and circulating system:**
A differential pressure gauge and a circulation system were attached to the column.
5) **Injection of de-aired water:**
De-aired water was injected from the lower part of the column using an HPLC pump or a screw pump at a constant rate for 16 hours. The injected water percolated through sand material and flowed into the circulating tank. While the water was circulated, the differential pressure between the inflow and outflow points was measured using the differential pressure gauge.

6) **CT scan after water injection:**
The measuring system and the circulation system were removed after injecting water. Finally, the column was scanned using the microfocus X-ray CT scanner.

7) **Increasing injection rate:**
The injection rate was increased, and steps (3) to (6) were repeated.

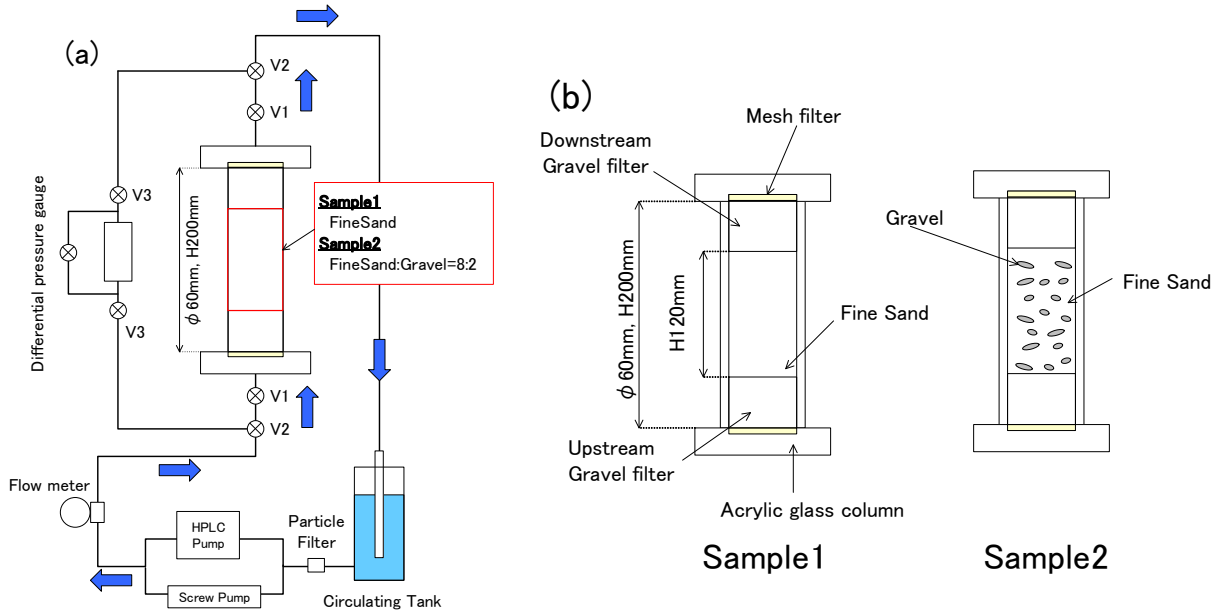

Figure 2. Schematic representation of experimental apparatus

(a): experimental apparatus. (b): illustration of experimental materials of Sample1 and Sample2.

2.3 CT SCANNING

CT scanning was performed using a TXS-CT 450/160 scanner at the Civil Engineering Research Laboratory at the Central Research Institute of Electric Power Industry. The microfocus X-ray CT scanner is shown in **Figure 3**. In this experiment, we used 160 kV X-ray sources, the maximum voltage of which is 160 kV, and the minimum focal spot size of 4 μm. A scanning energy of 150 kV with 350 μA was applied. A total of 3600 projections of 360° were measured, and the exposure time per projection was 800 ms. The pixel size was 50 μm/pixel, and the field of view per CT scan was approximately 100 mm. Hence, the CT scan was concluded two times and merged two CT images.

3. EXPERIMENTAL RESULTS

3.1 MEASUREMENT RESULTS OF DIFFERENTIAL PRESSURE

The measurement results of differential pressure and permeability for Sample1 and Sample2 at injection rates of 40 mL/min and 160 mL/min are shown in **Figure 4** and **Figure 5**, respectively. At the injection rate of 20 mL/min, the permeability of Sample1 was 1.85×10^{-4} m/s,

and the hydraulic gradient was 0.64, whereas the permeability of Sample2 was 2.34×10^{-4} m/s, and hydraulic gradient was 0.50. The permeability of Sample2 was thus slightly higher than that of Sample1. The differential pressure of both materials remains almost constant at injection rates below 40 mL/min (hydraulic gradient of Sample1 was 1.19 and that of Sample2 was 0.96). In contrast, the differential pressure changes only slightly at injection rates above 60 mL/min. At injection rates above 160 mL/min (hydraulic gradient of Sample1 was 4.56 and that of Sample2 was 3.90), the differential pressure changed significantly. It appears that soil particles were transported by seepage water flow, and the soil structure might have undergone some changes.

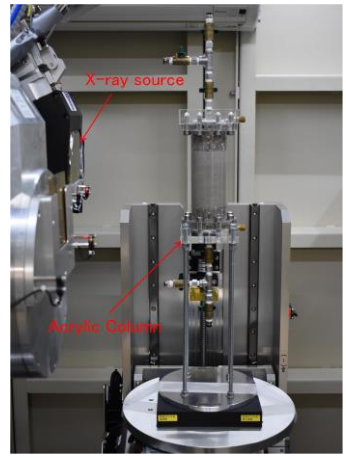

Figure 3. Snapshot of scanning acrylic column

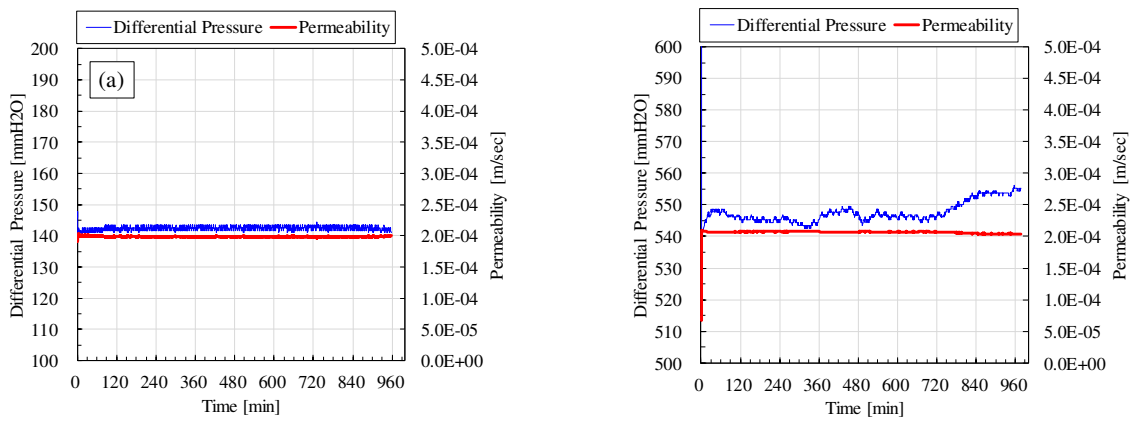

Figure 4. Differential pressure of Sample1 (fine sand)

(a): 40 mL/min injection rate. (b): 160 mL/min injection rate.

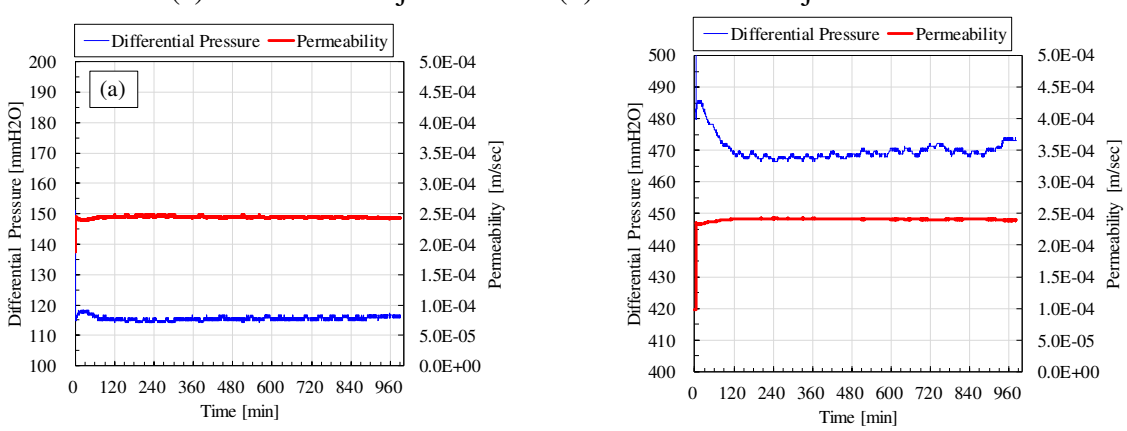

Figure 5. Differential pressure of Sample2 (mixture of fine sand and gravel)

(a): 40 mL/min injection rate. (b): 160 mL/min injection rate.

3.2 CT IMAGES

The CT scan images along the flow direction plane at injection rates of 40 mL/min and 160 mL/min are shown in **Figure 6** (Sample1) and **Figure 7** (Sample2). Stacked CT images (right side figure) are shown to emphasize the gray value contrast. A total of 100 sliced planes (5 mm thickness, 50 μm pixel size) were stacked along the view direction, and the minimum gray value is displayed onto one CT image. **Figure 8** shows the schematic view of stacked CT image.

Figure 6 and **Figure 7** show that fine sand particles were washed out into the downstream gravel filter at the injection rate of 160 mL/min. **Figure 9** (Sample2) shows that a crack occurred in the upstream part at 160 mL/min injection rate, and the crack clearly advanced along the flow direction at the 200 mL/min injection rate. This implies that the piping progression behavior in Sample1 (fine sand only) and Sample2 (mixture of fine sand and gravel) is different.

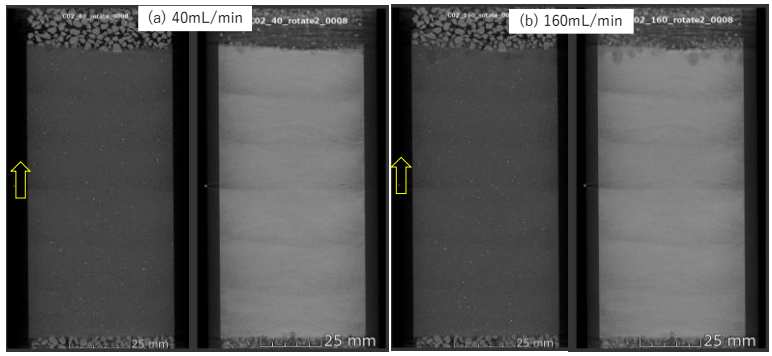

Figure 6. CT images of Sample1 (fine sand)

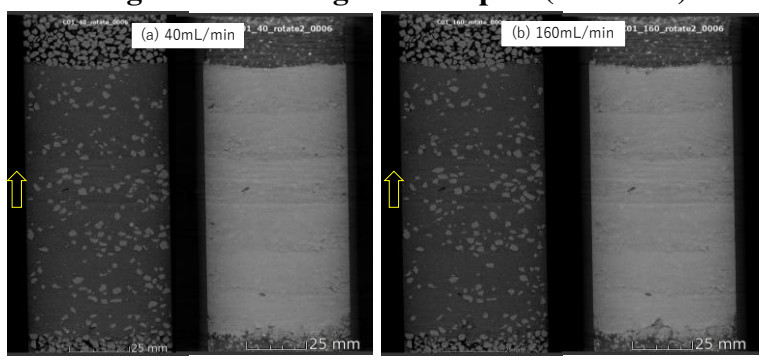

Figure 7. CT images of Sample2 (mixture of fine sand and gravel)

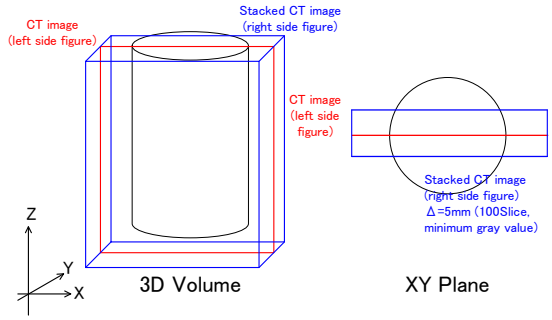

Figure 8. Schematic view of stacked CT image

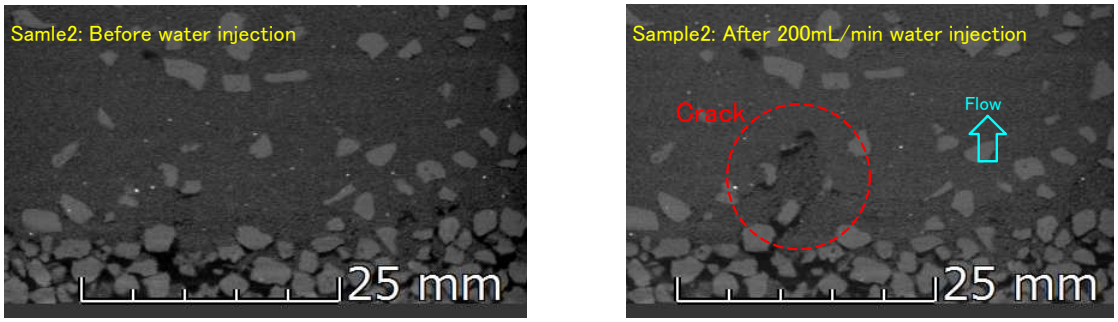

Figure 9. Enlarge CT image in upstream part (Sample2)

4. IMAGE ANALYSIS

We conducted image analysis, gray value analysis, and gravel-fabric analysis for each CT image and evaluated the changes in the internal structure of the soil.

4.1 GRAY VALUE ANALYSIS

The statistical analysis results of the gray value for each CT image are shown in **Table 1** and **Table 2**. We attempted to unify the operation procedure by warming-up the X-ray source before CT scanning or calibrating the X-ray detector. However, the measurement results of gray values obtained from scans of the same object remained slightly inconsistent. Therefore, CT images were normalized using Equation (1).

Table 1. Gray value analysis results of Sample1 (fine sand)

Injection rate [mL/min]	0	5	10	20	40	60	80	120	160	200
Min	0	0	0	0	0	0	0	0	0	0
Median	1944	1967	1842	1855	1969	1857	1715	1797	2101	2262
Max	64896	64896	64895	64896	64896	64895	64895	64895	64897	64898
Standard Deviation	925	970	895	898	946	906	833	883	987	1034

Table 2. Gray value analysis results of Sample2 (mixture of fine sand and gravel)

Injection rate [mL/min]	0	5	10	20	40	60	80	120	160	200
Min	0	0	0	0	0	0	0	0	0	0
Median	2891	3138	4802	3150	3017	16994	2383	2830	2985	2576
Max	64905	64907	65535	64907	64907	65047	64902	64906	64905	64904
Standard Deviation	1622	1703	2284	1680	1538	2149	1302	1458	1523	1318

$$I_i' = \frac{I_i - I_{mean}}{I_{std}} * I_{std}' + I_{mean}' \qquad (1)$$

where I_i depicts the pixel value before normalization; I_i' is the pixel value after normalization; $I_{mean}$is the average of the pixel value before normalization; I_{std} is the standard deviation of the pixel values before normalization; I_{mean}' is the average of pixel values after normalization, and I_{std}' is the standard deviation of pixel values after normalization. In this study, I_{mean}' and I_{std}' are 928 and 1931 for Sample1, and 1590 and 3066 at Sample2, respectively.

A schematic illustration of the gray value analysis is shown in **Figure 10(a)**. The gray value was analyzed for pixels positioned within 20 mm radius and 112 mm height from the center of the column. The number of layers was 198, and the vertical length of one layer was 0.55 mm.

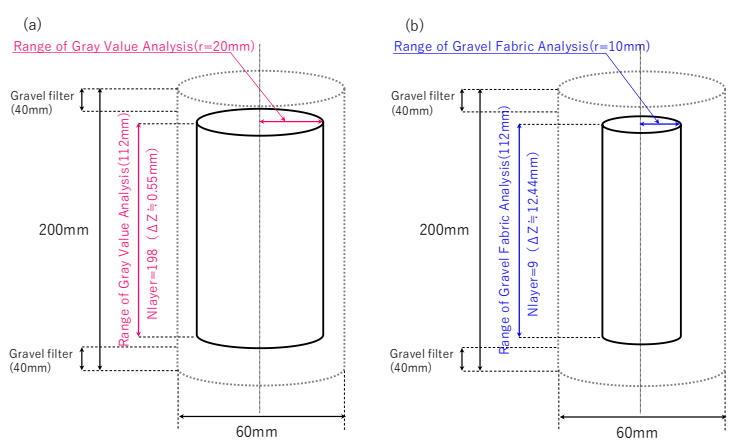

Figure 10. Schematic illustration of image analysis
(a): Gray value analysis (b): Gravel-fabric analysis

4.2 IMAGE SEGMENTATION AND GRAVEL-FABRIC ANALYSIS

Image segmentation that extracts pixels corresponding to gravel from the CT image in Sample2 was conducted before the gravel-fabric analysis. We used the image analysis software VGStudioMax and the Porosity/Inclusion Analysis Module. The procedure of image segmentation and gravel-fabric analysis is specified as follows:

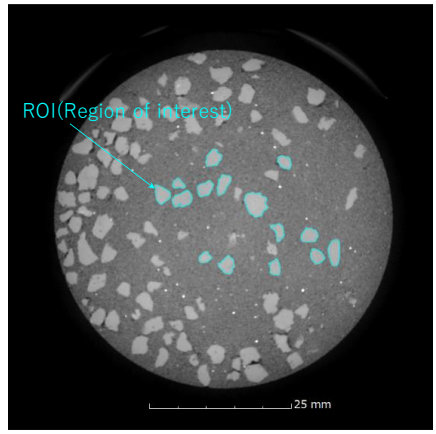

Figure 11. Snapshot of creating ROI using region growing from seed point

1) **Filtering of image**
   A median filter was applied to CT images to reduce noise. The filter size was three pixels.
2) **Creating ROI on XY plane**
   Fifteen gravels were manually identified using region growing tools to obtain the regions of interest (ROIs). The snapshot of creating a ROI is shown in **Figure 11**.
3) **Creating ROIs for all CT images**
   The gray values of the ROIs in step2 were analyzed, and the minimum and maximum gray values of gravel were noted. Subsequently, ROIs were constructed for all CT images by setting the relevant range of gray values.
4) **Labeling and fitting to ellipsoid**
   Each ROI was labeled and fitted to an ellipsoid. Finally, the deposition angle of the long-axis and the short-axis was calculated. In this study, 0° depicts the horizontal angle, and 90° denotes the vertical angle.

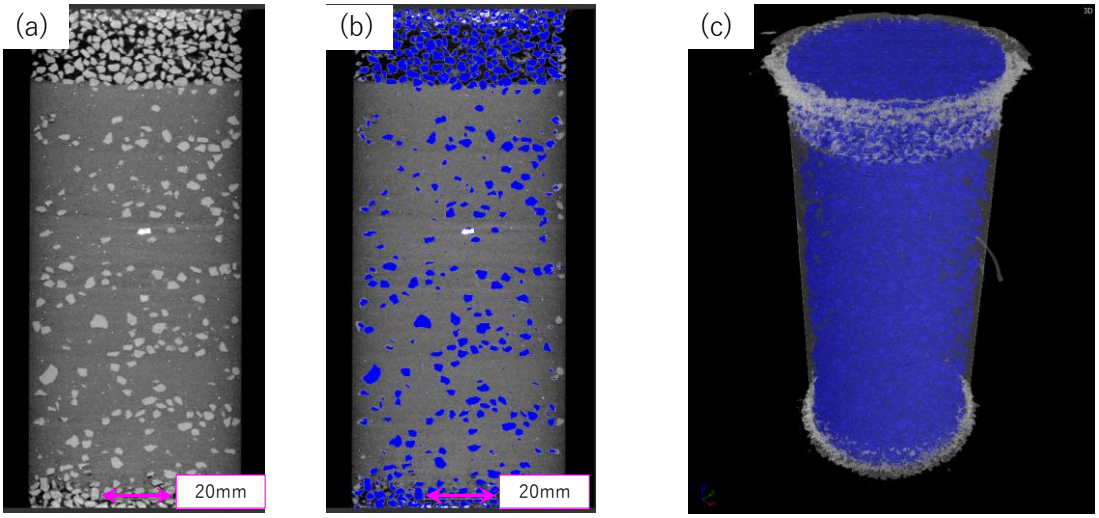

Figure 12. Snapshot of image segmentation

(a): CT images before segmentation. (b): CT images after segmentation. (c): CT images after segmentation in three-dimensional view.

The fabrics of gravels were analyzed for ROIs positioned within 10 mm radius and 112 mm height from the center of the column. The number of gravels used to analyze the fabric was ~360 per CT image. A snapshot showing the image segmentation is shown in **Figure 12**. Extracted gravels are colored-coded in blue.

4.3 IMAGE ANALYSIS RESULTS

Results of the gray value analysis are shown in **Figure 13** and **Figure 14**. The profiles of averaged gray values are plotted in both figures. In Sample1 (fine sand), the gray values decreased in the downstream part at injection rates greater than 160 mL/min. The lower gray values indicate a decrease in density. Therefore, soil particles were washed out by increasing the injection rate and decreasing the bulk density in the downstream part. In this setup, the vertical range of the gray value decline was about 20 mm. In Sample2 (fine sand and gravel), the decline in the downstream part was less than in Sample1. However, the gray values exhibited declines in the upstream part and in the middle stream part, to a lesser degree. In summary, piping progressed locally in mixture materials of fine sand and gravel.

The results of the gravel-fabric analysis are shown in **Figure 15**. By fitting each gravel to an ellipsoid, the average of the long-axis and short-axis dip angles were calculated every 12.4 mm (the number of layers is nine) and plotted accordingly. The maximum variation in the dip angle

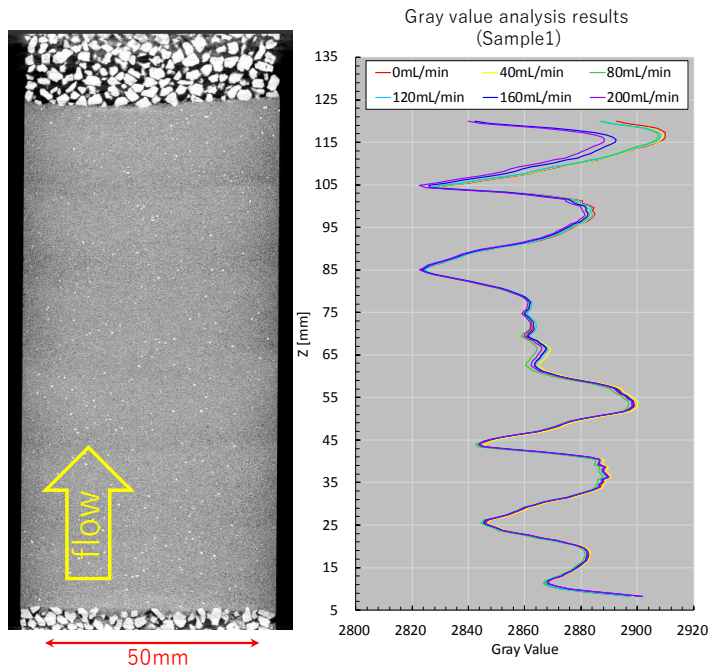

Figure 13. Gray value analysis results of Sample1 (fine sand)

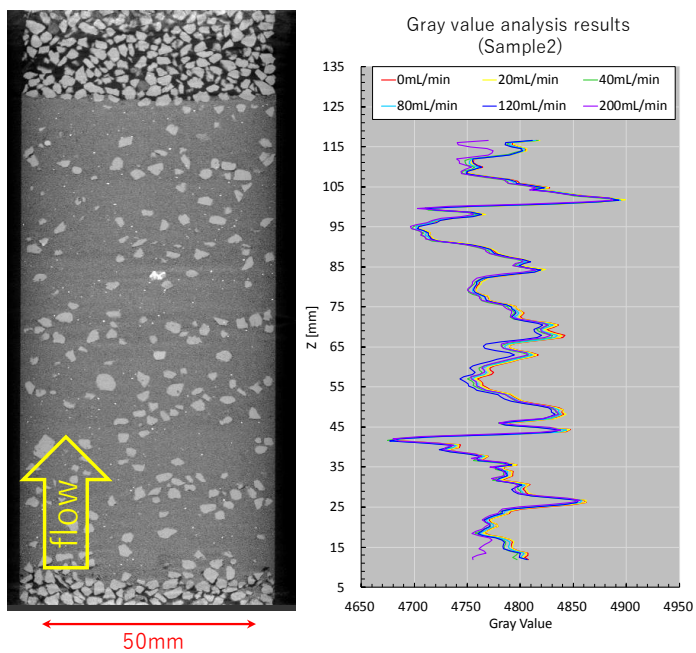

Figure 14. Gray value analysis results of Sample2 (mixture material of fine sand and gravel)

average was about 3° from these results. The ellipsoid fitting method performed on CT images might incur errors of 5° because of partial volume effects. Therefore, the attitudes of gravels were not almost change with percolating water and soil particles were washed out in local in this experiment.

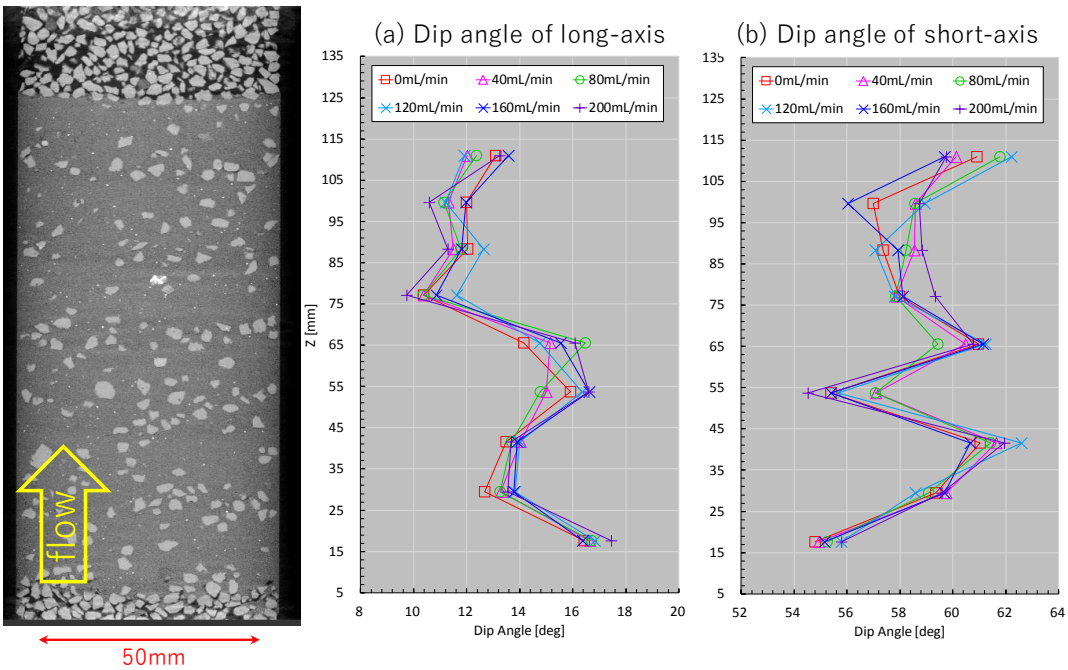

Figure 15. Gravel-fabric analysis results of Sample2.
(a): Dip angle of long-axis, (b): Dip angle of short-axis.

5. CONCLUSIONS

We investigated the progression of piping behavior in soils. To this end, 1D-column experiments were conducted with multistep water injection. We used two samples for the experiments, one with only fine sand (Sample1) and the other being a mixture of the fine sand and gravel (Sample2). CT scans were performed after water injection using a microfocus X-ray CT scanner. In this manner, the internal structure of soil was visualized without object destruction. From the acquired CT images, image analysis was conducted to evaluate the change in gray values and gravel fabric.

From the results obtained with Sample1 and Sample2, soil particles were observed to wash out in the downstream part. A crack also occurred in the upstream part and advanced along the flow direction with increasing water injection rate in Sample2. From the results of image analysis in both cases, the gray value decreased in the downstream part. Further, in Sample2, the gray value slightly changed in the middle stream part as well, whereas the fabric of gravel remained unchanged. Therefore, piping was also found to locally progress in the mixture material of fine sand and gravel.

REFERENCES

Richards, K.S. and Reddy, K.R. (2007). "Critical appraisal of piping phenomena in earth dams", *Bull Eng Geol Environ*, No.66, pp.381–402.

Pierson, T.C. (1983). "Soil pipe and slope stability", *Quarterly Journal of Engineering Geology*, Vol.16, pp.1–11.

Ke, L., and Takahashi, A. (2012). "Strength reduction of cohesionless soil due to internal erosion induced by one-dimensional upward seepage flow", *Soils and Foundations*, Vol.52, No.4, pp.698-711.

Wang, S., Chen, J., He, H. and He, W. (2016). "Experimental study on piping in sandy gravel foundations considering effect of overlying clay", *Water Science and Engineering*, Vol.9, No.2, pp.165-171.

Yang, K. and Wang, J. (2017). "Experiment and statistical assessment on piping failures in soils with different gradations", *Marine Georesources & Geotechnology*, Vol.35, No.4, pp.512-527.

Ketcham, R.A. and Carlson, W.D. (2001). "Acquisition, optimization and interpretation of X-ray computed tomographic imagery", Applications to the geosciences, *Computers and Geosciences*, Vol.27, No.4, pp.381-400.

Otani, J. and Obara, Y. (2003). "X-ray CT for geomaterials Soils, Concrete, Rocks".

Desrues, J., Viggiani, G. and Besuelle, P. (2006). "Advances in X-ray Tomography for Geomaterials".

Cnudde, V. and Boone, M.N. (2013). "High-resolution X-ray computed tomography in geosciences: A review of the current technology and applications, Earth-Science Reviews", No.123, pp.1-17.